Design of a Linear Transverse Flux Actuator

H. Vande Sande [1], G. Deliége [1], K. Hameyer [1]
H. Van Reusel [2], W. Aerts [2], H. De Coninck [2]

[1]Katholieke Universiteit Leuven
Dept. ESAT, Div. ELECTA
Kasteelpark Arenberg 10, B-3001 Heverlee-Leuven
phone: +32 16 32 10 20 – fax: +32 16 32 19 85
e-mail: hans.vandesande@esat.kuleuven.ac.be

[2]Philips Optical Storage
Industriezone Noord 1000-1920
Kempische Steenweg 293, B-3500 Hasselt, Belgium

***Abstract* — Transverse flux motors feature high force densities and hence compact designs. Unfortunately, their complex three-dimensional geometries hamper industrial series production. This is especially true when the machine's dimensions are very small. The numerical computation of a linear transverse flux actuator, which is simultaneously compact and manufacturable, is presented here. The use of powdered soft magnetic composites is appropriate for this application. The finite element method is used to calculate the forces, the inductance and the back-emf. The actuator is designed for high dynamic and accurate positioning.**

***Index Terms* — Actuators, Permanent magnet machines, Finite element methods.**

1. Transverse flux principle

In transverse flux machines, the magnetic flux approximately flows in planar surfaces perpendicular to the direction of motion of the moving part. This property enables a physical separation of the windings and the magnetic interaction region close to the mover (Fig. 1). Consequently, iron losses and Joule losses are independent from each other. When compared to other machine types, higher force densities are achievable, because the coil flux is linked to all the mover poles. By augmenting the number of poles per unit length, the force density is further increased without changing the current [5].

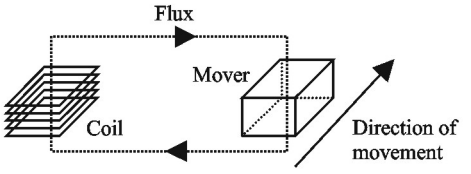

Fig. 1: Transverse flux principle.

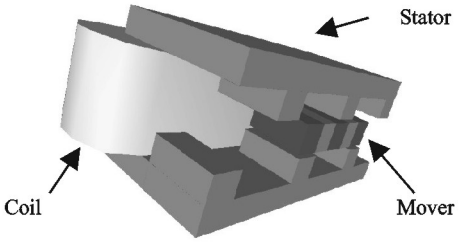

Fig. 2: Linear transverse flux actuator.

2. Linear transverse flux actuator

Figure 2 illustrates how to construct a linear transverse flux actuator applying the concept of figure 1. The mover comprises three high energy NdFeB-magnets magnetised in the direction of motion and two ferromagnetic connections representing the mover poles (Fig. 3). The configuration of the stator is more complicated, but it contains two of the same components (Fig. 4).

Powdered soft magnetic composites are particularly appropriate for this application, because the use of permanent magnets enlarges the airgap magnetically and hence reduces the relative importance of the powder material's permeability [1,2,3]. Furthermore, the basic stator component is easily formed in a die followed by a sintering process. This also permits industrial series production, even when the dimensions are very small.

3. Design specifications

The proposed device serves as an actuator. It is specified that the actuator must operate a mass m_{mover} over an averaged distance Δx_{avg} in a time Δt_{avg}. However, shorter or longer trajectories up to $3\Delta x_{\text{avg}}$ are possible and

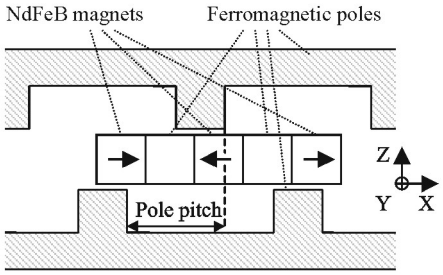

Fig. 3: Basic geometry of the transverse flux actuator.

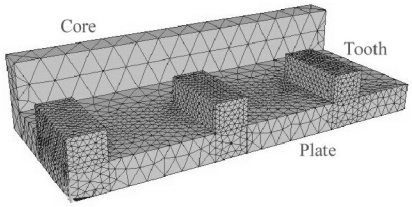

Fig. 4: Meshed basic component of the stator.

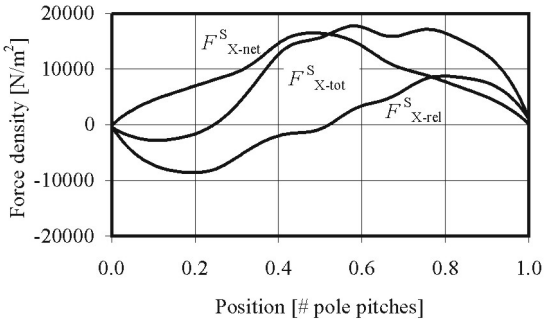

Fig. 5a: Position dependency of the x-component of the surface force density, for the geometry of figure 3.

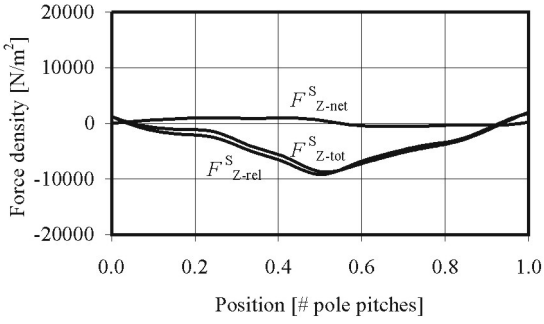

Fig. 5b: Position dependency of the z-component of the surface force density, for the geometry of figure 3.

the starting position is not fixed. It follows that a minimum acceleration a_{min} of

$$a_{\min} = 4\frac{\Delta x_{\text{avg}}}{\left(\Delta t_{\text{avg}}\right)^2} \tag{1}$$

must be attained over the first part of the trajectory Δx_{avg}, succeeded by a deceleration of $-a_{\min}$ over the second part. The actuator's height is restricted to $h_{\max}$. This eventually yields the following relation for the minimum surface force density $F^S_{\min}$ to be generated on the mover:

$$F^S_{\min} = \frac{\rho_{\text{mover}} f_h h_{\max} a_{\min}}{200} \quad , \tag{2}$$

in which ρ_{mover} is an equivalent mover mass density and f_h is the per cent ratio of the mover height to the actuator height.

The minimum surface force density for this application, considering the aforementioned specifications, equals 0.7 N/cm^2, assuming a mass density for the mover of 7800 kg/m^3 and an approximate per cent ratio f_h of 30. Obviously, the performance of the proposed actuator is not restricted by this condition, as transverse flux motors can generate force densities up to 4 N/cm^2 and even more [4,6]. Besides the surface force density specification, some other requirements have been determined in advance, among which a low force ripple, a high efficiency and a high ratio of the resulting force to the applied current over the whole length.

4. Fundamental behaviour

When the coil is not excited, reluctance forces drive the mover towards a position with a minimum of field energy. On the other hand, an extra force is generated upon the reluctance force when the coil is driven by a current. This additional force is called the net force. It depends on the applied current and the mover position. The total force is the sum of the reluctance force and the net force. All forces have an x-component in the direction of motion and a z-component along a vertical axis (Fig. 3). The y-component of the forces is not considered, as it remains small relative to the other components.

Here, the basic geometry from figure 3, for which all mover parts are of equal height and width, is considered. The analysis of this actuator requires a 3D-approach, due to the complexity of the flux patterns. The finite element method is used to study the fundamental behaviour of this device. Figure 4 shows the 3D mesh, which is obtained after applying solid modelling on one half of the stator. The mesh is strongly refined close to the teeth and the mover in order to obtain an accurate field solution around the mover. The forces are determined from this solution by further improving the accuracy of the local field around the mover using a local analytical solution of the Laplace equation [8,9].

The position-dependency of the surface force density components, for a constant current in the coil, is plotted in figures 5a and 5b. The position is expressed in terms of the number of pole pitches. One pole pitch τ is defined as the x-distance between two successive poles with different polarity. This is half of the distance between two poles on the same plate (Fig. 3).

The following symmetry conditions are applied to determine the forces outside the plotted domain:

$$\begin{aligned} F^S\left(\frac{x}{\tau}\right)\Big|_I &= F^S\left(\frac{x}{\tau}+2\right)\Big|_I \\ F^S\left(\frac{x|_{F=0}+\Delta x}{\tau}\right)\Big|_I &= -F^S\left(\frac{x|_{F=0}-\Delta x}{\tau}\right)\Big|_I \end{aligned} \quad . \tag{3}$$

From figures 5a and 5b, some important symmetry rules can be observed:

- $F^S_{\text{X-rel}}$ is periodic with period τ.
- $F^S_{\text{Z-rel}}$ is periodic with period 2τ.
- $F^S_{\text{X-net}}$ is periodic with period 2τ.
- $F^S_{\text{Z-net}}$ is negligible compared to $F^S_{\text{Z-rel}}$. Coil currents have almost no influence on the forces in the Z-direction.
- $F^S_{\text{X-rel}}$ and $F^S_{\text{Z-rel}}$ are of about the same magnitude.
- All reluctance and net forces can be approximated by a triangularly shaped periodic function.

It can be observed that, for a constant position and within the required specifications, the surface force density $F^S_{\text{X-net}}$ is proportional to the applied current. Hence, the proportionality factor is position dependent and behaves in the same way as the net surface force density.

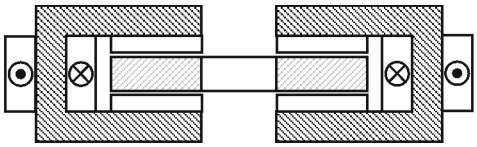

Fig. 6: Double motor concept: two parallel shifted motors with connected movers, featuring constant force generation and increased efficiency.

5. Double actuator requirement

It is impossible to generate a constant driving force in the direction of motion because zero-force positions appear along the trajectory. Moreover, holding the mover in a fixed position requires a constant current in the coil to compensate for the reluctance force. This yields very low efficiencies. These problems are solved by joining a second, identical actuator to the construction to form a double arrangement, without violating the maximum height specification (Fig. 6). A non-ferromagnetic material connects both movers. The second actuator is shifted relatively to the first motor over a distance of half a pole pitch, in order to obtain an approximately constant resulting net force in the direction of motion when both coils are driven by the same current.

By this shift, the reluctance forces in the direction of motion approximately compensate for each other. As a consequence, the mover can be held in a fixed position without significant currents in the coil. Unfortunately, the reluctance forces in the vertical direction do not compensate for each other. Moreover, the individual reluctance forces result in torques $T_{\text{X-rel}}$ and $T_{\text{Z-rel}}$ around the x and z-axis (Fig. 7). These must be covered entirely by the linear bearing.

6. Optimisation of the force characteristics

Two parameters are introduced in order to optimise the shape of the force characteristics: the skewing ratio f_{S} and the iron-magnet ratio f_{Fe}. Their physical meaning is illustrated in figure 8. Analogous to rotating permanent magnet devices, skewing reduces the reluctance force but it also reduces the obtainable net force. On the other hand, reducing the iron width w_{Fe} yields a higher net force, because the flux density in the mover iron increases when

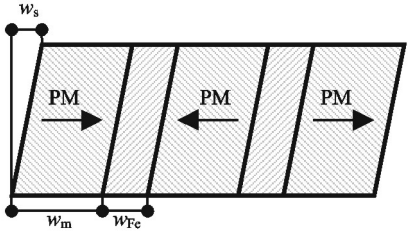

$$f_{\text{S}} = \frac{w_{\text{S}}}{w_{\text{m}}} \qquad f_{\text{Fe}} = \frac{w_{\text{Fe}}}{w_{\text{m}}}$$

Fig. 8: Physical meaning of the skewing ratio f_s and the iron-magnet ratio f_{Fe}.

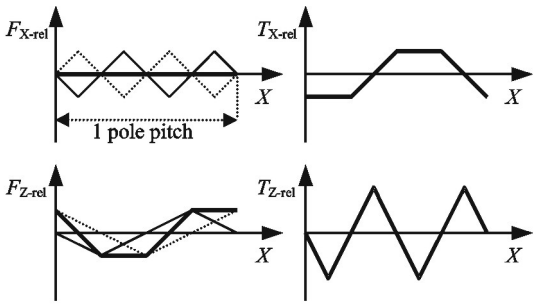

Fig. 7: Reluctance forces and torques appearing in the double motor arrangement, for a shift equal to half a pole pitch.

the iron width decreases. Hence, a better performance is obtained if skewing is combined with a decrease of the iron width. The effect of both parameters is expressed in terms of the flux linkage ξ

$$\xi(f_{\text{S}}, f_{\text{Fe}}) = \frac{\int_0^{\tau} F_{\text{net}}\,\mathrm{d}x \Big|_{f_{\text{S}};\, f_{\text{Fe}}}}{\int_0^{\tau} F_{\text{net}}\,\mathrm{d}x \Big|_{f_{\text{S}}=0;\, f_{\text{Fe}}}} \quad , \qquad (4)$$

and is plotted in figure 9 [7].

This figure is only valid if the current in the coil does not yield saturation of the mover iron. Under this condition, a still higher flux linkage can be obtained when a further iron-magnet ratio decrease is combined with a slight skewing ratio increase. However, to avoid a drop of the flux linkage if higher currents have to be applied, some margin is retained and both parameters are derived from the present optimum in figure 9: $f_{\text{S}} = 0.3$ and $f_{\text{Fe}} = 0.8$. The optimised characteristics are compared with the previous characteristics in figure 10. The net force has a better triangular shape than for the previous geometry, which is advantageous for control purposes.

7. Dynamic simulation modelling

Next to the determination and optimisation of the force characteristics, 3D finite element simulations are employed to model the dynamic behaviour of the actuator. By considering the magnetic equivalent circuit of the actuator, it is illustrated in which way the inductance and the

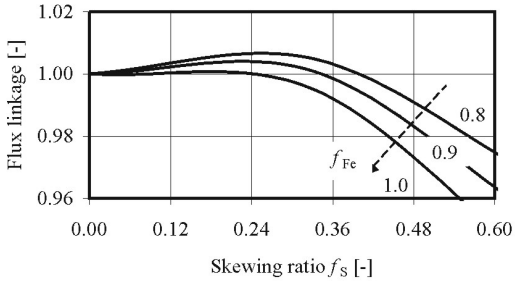

Fig. 9: Flux linkage dependency on the skewing ratio f_s and the iron-magnet ratio f_{Fe}.

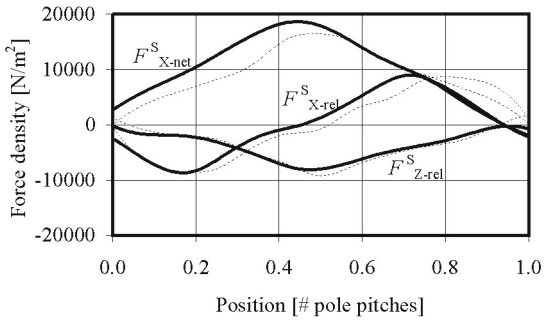

Fig. 10: Position dependency of the components of the surface force density, for the optimized geometry (bold line) and for the geometry of figure 3.

back-emf are computed numerically. As a result, all required parameters are known to perform a dynamic simulation of the behaviour including the PWM-control scheme.

A. Magnetic equivalent circuit

The magnetic field lines, forming a closed path, are represented by the magnetic equivalent circuit (MEC) of figure 11. Leakage flux is neglected in this study. If no current is applied to the coil, a flux ϕ_0 flows in the MEC, corresponding to the operation point p_0 on the demagnetisation characteristic of the NdFeB-magnets (figure 12). The value of the flux ϕ_0 depends on the position of the mover. If the coil is driven by a current, the operation point moves along the demagnetisation curve. The resulting flux change $\Delta\phi$ depends on the mover position, the sign and the magnitude of the current. The flux Ψ linked to the coil then equals

$$\begin{aligned}\psi &= N(\phi_0 + \Delta\phi) \\ &= N\phi_0 + Li\end{aligned} \quad , \tag{5}$$

with N the number of windings and L the inductance of the coil. When a voltage u is supplied to the coil with a resistance R, the following expression holds:

$$u = Ri + \frac{\mathrm{d}\psi}{\mathrm{d}t} \quad . \tag{6}$$

Combining these formulas yields

$$\begin{aligned}u &= Ri + L\frac{\mathrm{d}i}{\mathrm{d}t} + i\frac{\mathrm{d}L}{\mathrm{d}t} + N\frac{\mathrm{d}\phi_0}{\mathrm{d}t} \\ &= Ri + L\frac{\mathrm{d}i}{\mathrm{d}t} + iv\frac{\mathrm{d}L}{\mathrm{d}x} + Nv\frac{\mathrm{d}\phi_0}{\mathrm{d}x}\end{aligned} \quad . \tag{7}$$

with v the velocity of the mover.

B. Energy considerations

The inductance L of the coil, for a fixed position of the mover, is computed by:

$$L = 2\frac{(w_{tot} - w_0)}{i^2} \quad . \tag{8}$$

The energy w_0 corresponds to the energy in the airgap due to the presence of the permanent magnets. The energy w_{tot} is the energy in the airgap when a current is applied to the coil. Both quantities are obtained from the 3D finite element computation. It can be observed that the position dependency of the inductance is very small. This is due to the use of NdFeB-magnets, which in magnetic terms behave like air, because their differential relative permeability approximates unity. If eq. 8 is derived with respect to the position, an equation relating dL/dx to F_{net} is obtained:

$$\begin{aligned}\frac{\mathrm{d}L}{\mathrm{d}x} &= \frac{2}{i^2}\left(\frac{\mathrm{d}w_{\mathrm{tot}}}{\mathrm{d}x} - \frac{\mathrm{d}w_0}{\mathrm{d}x}\right) \\ &= \frac{2}{i^2}(F_{\mathrm{tot}} - F_{\mathrm{rel}}) \\ &= \frac{2}{i^2}F_{\mathrm{net}}\end{aligned} \quad . \tag{9}$$

By considering the energy w_0 in the airgap due to the presence of permanent magnets, a more relevant expression for dϕ_0/dx is obtained. From figure 12 it follows that the flux density B_0 and the field strength H_0 in the magnet are linear functions of a parameter α:

$$B_0 = (1-\alpha)B_r \quad , \tag{10}$$

$$H_0 = \alpha H_c \quad , \tag{11}$$

with B_r and H_c the remanent and coercive field respectively. These equations only hold for magnets having a linear demagnetisation characteristic, such as the NdFeB-magnets considered here. The energy w_0 is proportional to the surface of the shaded area (figure 12).

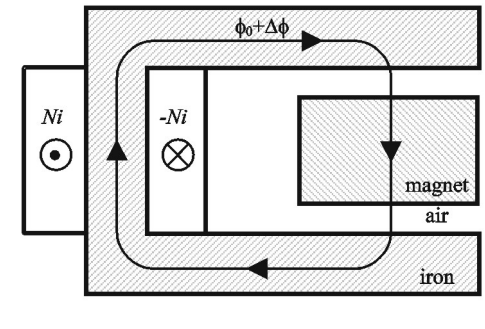

Fig. 11: Idealised magnetic equivalent circuit of the actuator.

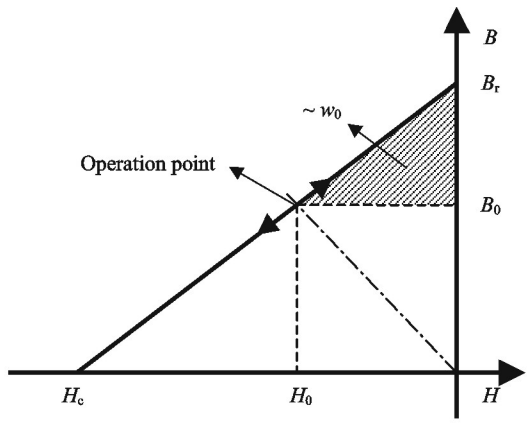

Fig. 12: Typical demagnetisation characteristic of NdFeB-magnets.

Hence

$$w_0 \sim \alpha^2 B_r |H_c| \quad \Rightarrow w_0 = \alpha^2 w_0^{max} \quad , \qquad (12)$$

with w_0^{max} the energy corresponding to the entire surface below the demagnetisation curve in the second quadrant. As the flux ϕ_0 is the product of B_0 and the magnet's surface S, it follows that

$$\frac{d\phi_0}{dx} = -\frac{B_r S}{2\sqrt{w_0^{max}}} \cdot \frac{1}{\sqrt{w_0}} \cdot \frac{dw_0}{dx} = -\frac{B_r S}{2\sqrt{w_0^{max}}} \cdot \frac{F_{rel}}{\sqrt{w_0}} \quad . \qquad (13)$$

C. Simulation scheme

Combining equation (7), (9) and (13) together with the equation of motion for the mover leads to a coupled set of differential equations, which describe the dynamical behaviour of the linear actuator:

$$u = Ri + L\frac{di}{dt} + 2\frac{v}{i}F_{net} - \frac{B_r SN}{2\sqrt{w_0^{max}}} \cdot \frac{v}{\sqrt{w_0}} F_{rel} \quad , \qquad (14)$$

$$F_{net} = m\frac{d^2x}{dt^2} + c_f \frac{dx}{dt} + kx \quad , \qquad (15)$$

with c_f the mechanical friction and k the mechanical damping on the mover. Both equations consider one part of the actuator. The last two terms in (14) represent a voltage drop caused by the velocity of the mover and can be considered as the back-emf. This formula is only valid as long as no saturation occurs in the actuator. Equations (14) and (15) can directly be implemented in a simulation scheme for the controller design. The quantities F_{rel}, w_0 and L only depend on the mover's position. The net force depends on both, the position of the mover and the current in the coil. These dependencies can be incorporated in the dynamical simulation scheme by means of look-up tables.

8. Conclusions

The analysis of a linear transverse flux actuator for fast positioning is presented. The transverse flux concept allows for high force densities and a compact actuator design. Powdered soft magnetic composite materials are particularly interesting for this type of application. The finite element method is applied to the 3D-model, generated by solid modelling techniques. The solver directly computes the stored energy in the model. The forces are computed in a post-processing step, by further improving the accuracy of the local field around the mover using a local analytical solution of the Laplace equation. To avoid zero-force positions, a second actuator is joined and is shifted relatively to the first one over half a pole pitch. The resulting forces and torques have to be covered by the linear bearings. It is shown that combining the effect of skewing and iron width adaptation can increase the obtainable net force. An analytical model for the dynamical behaviour of the actuator, based on a magnetic equivalent circuit, is presented. The parameters of this model are obtained by finite element computations.

Acknowledgment

The authors are grateful to the Belgian "Fonds voor Wetenschappelijk Onderzoek Vlaanderen" for its financial support of this work and the Belgian Ministry of Scientific Research for granting the IUAP No. P4/20 on Coupled Problems in Electromagnetic Systems. The research Council of the K.U.Leuven supports the basic numerical research.

References

[1] P. Jansson, M. Persson, A.G. Jack and B.C. Mecrow, "Powdered soft magnetic materials for medium frequencu applications," *Proc. Soft Magnetic Materials SMM'96*, February 1996.

[2] B.C. Mecrow, A.G. Jack and S.A. Evans, "Permanent magnet machines with soft magnetic composite stators," *Proc. ICEM'98*, pp. 346-351, September 1998.

[3] Ö. Krogen and A.G. Jack, "Insulated iron powder (SMC) used as soft magnetic material in a rotating electrical machine," *Proc. Metallurgy World*, November 2000.

[4] M. Bork and G. Henneberger, "New transverse flux motor concept for an electric vehicle drive system," *Proc. ICEM'96*, pp. 308-313, September 1996.

[5] R. Blissenbach and G. Henneberger, "Numerical calculation of 3D eddy current fields in transverse flux machines with time stepping procedures," *COMPEL*, Vol. 20, N0. 1, pp.152-166 2001.

[6] H. Weh, "Transverse flux (TF) machines in drive and generator application," *Proc. Stockholm Power Tech Conference*, pp. 75-80, June 1995.

[7] R. Kruse, "Calculation methods for a transverse flux motor," *CD-Proc. OPTIM'00*, May 2000.

[8] K. Hameyer, R. Mertens, U. Pahner and R. Belmans, "New technique to enhance the accuracy of 2D/3D field quantities and forces obtained by standard finite-element solutions," *IEE Proc.-Sci. Meas. Technol.*, Vol. 45, No. 2, pp. 67-75, March 1998.

[9] R Mertens, R. De Weerdt, U. Pahner and K. Hameyer, "Force calculation based on a local solution of Laplace's equation," *Proc. CEFC'96*, pp. 354, March 1996.